Observation of High Enegy γ-rays with Large-Area Emulsion Chamber at Mt. Fuji

AUTHOR(S):

Torii, Shoji

CITATION:

Torii, Shoji. Observation of High Enegy γ-rays with Large-Area Emulsion Chamber at Mt. Fuji. Memoirs of the Faculty of Science, Kyoto University. Series of physics, astrophysics, geophysics and chemistry 1977, 35(1): 109-129

ISSUE DATE:

1977-09

URL:

http://hdl.handle.net/2433/257560

Memoirs of the Faculty of Science, Kyoto University, Series of Physics, Astrophysics, Geophysics and Chemistry, Vol. XXXV, No. 1, Articles 7, 1977.

OBSERVATION OF HIGH ENEGY γ-RAYS WITH LARGE-AREA EMULSION CHAMBER AT MT. FUJI

By

Shoji TORII

Department of Physics, Faculty of Science, Kyoto University, Kyoto

(Received June 9, 1975)

ABSTRACT

The flux and energy spectrum have been obtained of cosmic-ray electromagnetic component (γ-rays) in the energy region 1.5 TeV $-$100 TeV by use of a large-area (134.4 m^2) emulsion chamber F IV exposed at the top of Mt. Fuji (650 g/cm^2 atmospheric depth) for 317 days. The chamber consisted of a thin part (132 m^2) of 6 cascade units thick (Pb) and a thick part (2.4 m^2) of 14 cascade units thick. The spectrum obtained from the thin part ranges from 15 TeV to 100 TeV. It is consistent with that obtained with better accuracy from the thick part, which covers the energy region 1.5 TeV $-$20 TeV.

The spectrum can be expressed by $(5.9\times10^{-10}/\mathrm{cm}^2\cdot\mathrm{sec}\cdot\mathrm{str})\times(\mathrm{E}/1.5\ \mathrm{TeV})^{-\beta}$ with $\beta=2.0\pm0.1$. The integral zenith angle distribution of the γ-rays is expressed by $\cos^n\theta$ with $n=9.0\pm0.1$.

In the thin part, methods have been introduced which enable us to determine the γ-ray energy by observing early stages of shower development. It is shown that the methods give the energy of showers within 30% error as compared with one determined by the usual methods (used for the thick part) in which the whole transition of the shower is employed.

Comparing the result with other experimental results, breif discussions are given on the cross section of cosmic-ray nucleons with air nuclei and the scaling law of the energy distribution for the multi-particle production.

1. Introduction

Emulsion chamber (EC) with X-ray film is superior to conventional electric detectors in space resolution ($\sim$200 μm) and in energy determination of high energy ($\gtrsim$1 TeV) electromagnetic particles (hereafter abbreviated as γ-rays). These characteristics are suitable for the observation of the core of extensive air showers (EAS) which might reflect directly the nature of multi-particle productions at very high energy ($\gtrsim$100 TeV) collisions of cosmic-ray nucleons with air nuclei.

The purpose of the Fuji large-area emulsion chamber project[1] is to study the core structure and the morphorogical characteristics of EAS.

To catch 'γ-ray family' with energy as high as possible, the chambers were constructed at the top of Mt. Fuji and the area was expanded as wide as possible. The thickness of shower producing material (Pb) was not enough to observe the development of electromagnetic cascade shower to the end. So the shower energy

must be determined only with the information of the early stage of shower development. To aid the scanning and the energy determination of numerous showers in a large area, industrial X-ray films have been employed. For the energy determination of a given shower, the optical densities of shower spots registered on X-ray films at different depths were measured with the photometer under different slit sizes. Nuclear emulsion has been employed only for the energy calibration.

In this paper, we present mainly a result of the Chamber F IV among the Chambers F I–F VI. As a first step of the experiment, we obtained the flux, the energy spectrum and the zenith angle distribution of γ-rays up to 100 TeV.

Section 2 gives a short description of the desing of the Chamber F IV and the method of shower detection. In §3, we present the method of energy determination and the accuracy. Considering many biases and corrections in the thin part, the flux and energy spectrum are obtained in the region 15 TeV–100 TeV, in §4. They are compared with those obtained in the thick part in the region 1.5 TeV–20 TeV. Finally, in Section 5 comparing with other experimental results, some problems about the multi-particle produtcion in our energy region are breifly discussed.

2. Design of chambers and method of detection[2)]

2–1 Design of the emulsion chambers

Table 1 shows the list of series of EC's exposed at the top of Mt. Fuji (3700 m above sea level and 650 g/cm^2 atmospheric depth). The Chamber F IV, of which result we present in this paper, was exposed for 317 days and consisted of two parts: one a thin type chamber of large area (6 cascade unit (c.u.) in thickness and 132 m^2 in area) and the other a thick type chamber of small area (14 c.u. in thickness and 2.4 m^2 in area).

The thick part was designed for the energy calibration and the observation of lower energy γ-rays, and it contained the photo-sensitive layers at every 2 c.u.

Table 1. Exposure list of chambers

Chamber	Exposure			Area	Thickness	Sensitive layers	Thick part
	From	To	Days	(M^2)	(C.U.)		(M^2)
FI	'68.9.19	'69.8.3	319	1.6	50	$E+2N+R$ at every 2 c.u.	
FII	'69.9.22	'70.7.1	282	40.0	4	$2N+R$ at 4 c.u.	
FIII	'70.9.13	'71.7.8	299	144.8	4	$N+R+F$ at 4 c.u.	1.2
FIV	'71.8.23	'72.7.5	317	134.4	6	N at 4 c.u., $N+R$ at 6 c.u.	2. 4
FV	'72.8.18	'73.7.7	324	132.0	6	$N+R$ at 4,6 c.u.	2.4
FVI	'73.8.3	'74.7.24	356	117.6	8 (10)	$N+R$ at 4,6,8, (10) c.u.	2 .4

E: Nuclear emulsion plate (Fuji ET-7B) N: X-ray film (Sakura Type-N)
R: X-ray film (Sakura Type-RR) F: X-ray film (Fuji #200)

from 4 c.u. to 14 c.u. from the top. Each layer was made up of a nuclear emulsion plate (FUJI ET7B) and three sheets of industrial X-ray films (one SAKURA Type-RR and two Type-N's). The photo-sensitive layers in the thin part consisted of only X-ray films (one Type-N at 4 c.u., one Type-N and one Type-RR at 6 c.u.).

The characteristics of the photo-sensitive materials and their development conditions are shown in Tables 2 and 3.

Table 2. Specifications of the sensitive materials

Type of emulsion	Emulsion thickness (Microns)	Grain size after development (Microns)	Base thickness (Microns)
Type-*N*	17.5	25	185
Type-*RR*	15.0	1.6	185
ET-7B!	50.0	0.7	1600

! Emulsion coated only one side of a base

Table 3. Development conditions of the sensitive materials

3-1. FUJI ET7B nuclear emulsion plate

	Temperature (°C)	Time (min.)	Chemicals
Pre-soaking	20	10	Tap water
Development	20	20	Amidol
Stop	20	5	Acetic acid
Fixing	20	90	Hypo
Washing	Natural	180	Tap water

3-2. SUKURA Type-N, RR X-ray films

	Temperature (°C)	Time (min.)	Chemicals
Development	20	11	Konidor-X
Stop	20	5	Acetic acid
Fixing	20	10	Konifix rapid
Washing	Natural	60	Tap water

2-2 Detection of events

In the thick part, we scanned the X-ray films for dark spots caused by γ-ray-initiated cascade showers. Then we looked for the corresponding shower tracks in the emulsion plates under the microscope. In the thin part, we scanned only the X-ray films. The detection threshold energy of showers is much higher (10 TeV) than that in the thick part because of lack of emulsion plates and insufficient thickness of shower producing materials.

2-3 Measurement of the zenith angle

The zenith angle of a detected shower was determined by measuring the displacement of the shower spots on the both sides of X-ray films (Type-RR). Then the angle θ was obtained by the relation $m=\tan\theta=d/a$, where a is the effective

thickness of film base, d is the horizontally projected displacement of the shower spots. The horizontal displacement was determined with $\pm 10\,\mu$m error because of the extension of shower spots and a is $200\,\mu\text{m}\pm 5\,\mu$m, so m was determined within absolute error of ± 0.05.

3. Energy determination of showers

3-1 Thick part

In the thick part, the energy of a shower was determined as follows. In every nuclear emulsion plate, the number of shower electrons within a certain radius from the shower axis was counted under the microscope and the transition of the number with depth (shower curve) was compared with the theoretical shower curves of given energies (see Fig. 1). At the same time the micro-photometry measurement[3] was done for the corresponding dark spots on the X-ray films with a square slit of $200\,\mu\text{m}\times 200\,\mu$m for Type-N, and $30\,\mu\text{m}\times 30\,\mu$m for Type-RR. This measurement gave the optical density D defined as $D=\log_{10}(I/I_0)$ where I is the intensity of light transmitted through a spot area on the film and I_0 is the light intensity through a general background field.

From the measurements the $D_{\max}-E_c$ relation was established, where $D_{\max}$

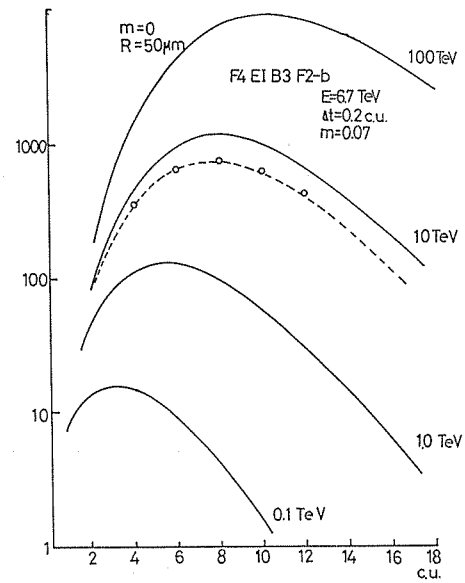

Fig. 1. Theoretical transition curves of the shower electrons and an example of the fitting of an observed shower in the thick part. Theoretical curves are for the energies of 0.1 TeV, 1.0 TeV, 10 TeV, and 100 TeV and for vertical incidence ($m=\tan\theta=0$).
Ordinate is the total number of electron tracks within a circle of radius $R=50\,\mu$m from the shower axis. The open circles are the measured results of the shower, coming with a zenith angle of $m=\tan\theta=0.07$. Abscissa is shifted horizontally by Δt to fit the measurement values to the theoretical ones. Dotted line is a best fit curve for the shower transition and the Δt is 0.2 c.u.. Thus we obtain the energy 6.7 TeV for the shower with the event number F4E1B3-F2-b.

and E_c were the maximum optical density of the shower spots and the energy of the shower determined by the counting method. Figure 2 shows the result: $D_{max}=0.14\times E_c^{0.85\pm0.05}$. Once the relation is established, the absolute value of the transition curve of D's is fixed for each energy and the basic information is obtained for the energy determination in the thin part. Figure 3 shows the theoretical curves for the transition of D's and some examples of energy determination of showers by the photometric method.

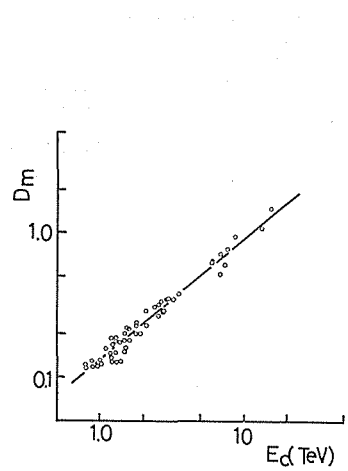

Fig. 2

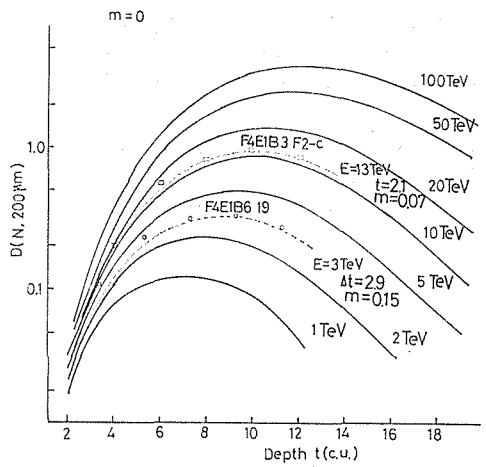

Fig. 3

Fig. 2. Relation of energy, E_c, obtained by counting method (see Fig. 1) and maximum optical density, D_m, for the showers with $m=\tan\theta$ smaller than 0.2. Photometric measurements were done with 200 μm $\times$ 200 μm square slit. The open circles are the measured results and the solid line represents a best fit curve: $D_m=0.14\times E_c^{0.85}$.

Fig. 3. Theoretical transition curves of the optical densities for the energies of 1 TeV, 2 TeV, 5 TeV, 10 TeV, 20 TeV, 50 TeV and 100 TeV and for vertical incidence, and examples of the fitting of the observed showers in the thick part. Ordinate is the opical density of shower spot measured with 200 μm $\times$ 200 μm squre slit. The open squares and circles are the measured optical densities of the showers with the event numbers F4E1B3-F2-c and F4E1B6-19, respectively. The event F4E1B3-F2-c has $\Delta t=2.1$ c.u. and $m=0.07$ and the energy determined by counting method is 13 TeV. And the event F4E1B6-19 has $\Delta t=2.9$ c.u. and $m=0.15$ and the energy is 3 TeV. Dotted lines are the best fit curves for each showers.

3–2 Thin part

For the energy determination in the thin part, neither the counting method nor the $D_{max}-E_c$ relation are applicable as mentioned earlier (§2–2). Because the shower curve is a function of the initial electron or photon energy E_0, the distance from the shower axis r and the depth t, the energy of a shower can in principle be determined if we know two different D's of a shower, such as D's under different depths measured with the same slit size or D's under different slit sizes. Besides the energy, we can know the starting point of the shower, which we represent by the depth Δt as measured from the top of the chamber.

3-2-1 Practical method

If more information than two D's is available, the accuracy of energy determination will be increased. Figure 4 shows an example of the diagram which has been employed in the parctical energy determination. In this case, the D's under 4 c.u. and 6 c.u. were measured on Type-N and Type-RR with considerably different slit sizes relevant to their sensitivities. They are denoted by D_6(N, 200), D_4(N, 200) and D_6(RR, 30), where $D_t(A, \mathrm{R})$ means the optical density measured with an R μm square slit on Type-A X-ray film under t c.u.. Then, from the relation determined by D_6(RR, 30) vs. D_4(N, 200)/D_6(N, 200), we obtain the energy and the Δt. The choice of the slit size and the type of films depend on the situation. For example, in case where another shower interferes within a slit area, the photometric measurement with this slit size is meaningless; the smaller size is required, but the measurement on Type-N with the slit size as small as 30 μm $\times$ 30 μm is irrelevant because the size of its silver grains is 5 μm—7 μm. Hence, measurements on Type-RR with different slit sizes are inevitable.

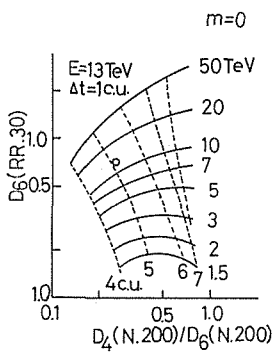

Fig. 4

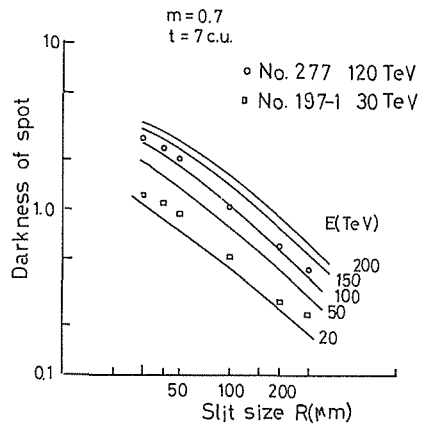

Fig. 5

Fig. 4. Theoretical curves for the relation between the $D_6(RR, 30)$ and the $D_4(N, 200)/D_6(N, 200)$ for the vertically incident shower ($m=\tan\theta=0$). (Spacing factor is not calibrated. See later.)
Solid and dotted lines represent the energy of showers and the depth of the observation point for the showers, respectively. An example of the fitting of an observed shower in the thin part is also shown. The open circles a measured result of a vertically incident shower. The difference between the depths obtained by the fitting, 5 c.u., and of the observation point, 6 c.u., gives the starting point depth, $\Delta t=1$ c.u.. And the energy is 13 TeV.

Fig. 5. Theoretical curves of the correlation of the optical densities and the slit sizes of photometric measurement (Type-*RR* film) and examples of the fitting of observed showers in the thin part. (Spacing factor is not calibrated. See later.)
The optical density is defined for the shower with the zenith angle $m=\tan\theta=0.7$ at the 7 c.u. vertical depth. The solid lines represent the theoretical curves for the shower with energies, 20 TeV, 50 TeV, 100 TeV, 150 TeV and 200 TeV. The open circles and squares are the measured optical densities of showers and the energies are given by 120 TeV for the shower with event number 277 and by 30 TeV for the shower with event number 197-1.

3-2-2 Comparision with other methods

The energy of showers was also determined by measuring D's on type-RR under 6 c.u. with square slits 30 μm, 40 μm, 50 μm, 100 μm, 200 μm and 300 μm. Figure 5 shows calculated curves and examples of energy determination. Another method for energy determination is to use the knowledge of the starting point and one D of a given shower. In Table 4, energies of 10 showers determined by the above three methods are listed. There is no systematic deviation among these.

Table 4. Comparision of shower energies determined by the different methods. (Spacing factor is not calibrated. See later.)

Event No. \ Method	A	B	C
No. 197-1	30 (TeV)	30	30
197-2	20	20	40
254	70	70	80
277	130	120	110
415	35	40	20
512	40	40	50
527	15	15	10
538	70	70	90
569	40	30	20
585	40	40	30

Method A: Relation of $D_4(N, 200)/D_6(N, 200)$ and the $D_6(RR, 30)$ (see Fig. 4).
Method B: $D_6(RR, R)$ with the various slit sizes, R μm: 30 μm, 40 μm, 50 μm, 100 μm and 200 μm (see Fig. 5).
Method C: $D_6(N, 300)$ for the known At measured by Method A or B.

3-2-3 Accuracy of the method

For showers observed in the thick part, the energies determined by the present method can be compared with those determined by the $D_{max}-E_c$ relation. As seen from Fig. 6 they are consistent within 30% error and no systematic errors are found.

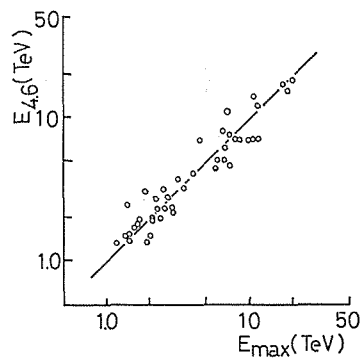

Fig. 6. Experimental result for the relation of energy, E_{max}, obtained by the relation $D_{max}-E_c$ (see Fig. 2) and that, $E_{4.6}$, by the relation $D_6(RR, 30)$-$D_4(N, 200)/D_6(N, 200)$ (see Fig. 4). The open circles are measured ones of the showers observed in the thick part.

3-2-4 Spacing effect[4]

In EC, the lateral spread of electron shower becomes larger than that of shower in pure lead. This effect is known as the 'spacing effect'.

In our chamber, the thin part lacks the emulsion plate which has the thickness 1600 μm. The theoretical shower curves (Fig. 1) are for the thick part, so they must be calibrated for the thin part. The calibration factor of energy for pure lead chamber is called as 'spacing factor', and the factor might be given 1.25 for the thin part and 1.45 for the thick part approximately. Then the ratio 0.86 will give the calibration fcator for the thin part, so we should reduce the energy by about 14%.

The discussion mentioned above is rather qualitative and a quantitative treatment is now in progress by the method of Monte-Calro simulation and we neglect the spacing effect in the present paper except for the absolute flux value.

4. Flux and energy spectrum of γ-rays

4-1 Thick part
—Energy region from 1.5 TeV to 20 TeV—

4-1-1 The ratio a of the flux of γ-rays to the flux of showers induced by nuclear active particles (Pb-jets)

The showers observed in EC are produced either by γ-rays or by nuclear active particles. In lead, the intensity of γ-rays attenuates as $\exp(-t)$* and that of Pb-jets as $\exp(-t/30)$ approximately**. This difference makes it possible to separate the γ-rays and the Pb-jets statistically.

The true distribution of the starting points of showers produced by particles with attenuation mean free path λ_a is $e^{-t/\lambda_a}(dt/\lambda_a)$. The real starting point distribution would be affected by the fluctuation of shower development as well as by errors in the measurement, because the starting points were estimated by the comparision with the transition curve of the shower theory in which the fluctuation is not involved. The probability that a shower with the true starting point t' is estimated to have a starting point t is found experimentally to be well approximated by a Gaussian distribution $(1/\sqrt{2\sigma\pi})\exp\{-(t-t')^2/2\sigma^2\}$. Then the real distribution of the starting point t is

$$dt\int e^{-t'/\lambda_a}\frac{dt'}{\lambda_a}\frac{1}{\sqrt{2\pi}\sigma}\exp\{-(t-t')^2/2\sigma^2\}$$
$$=\frac{dt}{\lambda_a}e^{-t/\lambda_a}e^{-\sigma^2/2\lambda_a^2}\Phi(t'/\sigma-\sigma/\lambda_a)$$

$$\text{, where } \Phi(x)=\frac{1}{\sqrt{2\pi}}\int_{-\infty}^{x}e^{-y^2/2}dy\,.$$

In Fig. 7, we give the results for $\sigma^2=3$ in the two cases of $\lambda_a=1$ for γ-rays,

---

* in c.u.

** The value of the attenuation mean free path of nuclear active particles in lead was measured with very thick EC and found to be about 30 c.u.[5]. A.P. Chubenko et al.[6] also measured the interaction cross section of nuclearactive particles with the mean energy 5 TeV by the calorimeter with lead and reported the cross section of 1810±110 mb which corresponds to $\lambda_a=34\pm2$ c.u.

and of $\lambda_a=30$ for Pb-jets. If the α at the top of chamber is known, we can give the attenuation behavior of the total showers in the chamber. As shown in Fig. 7, α is 2.0 ± 0.5. The α was given by 1.79 ± 0.25 at Mt. Chacaltaya[7] (the altitude 5200 m above sea level and the atomospheric depth 540 g/cm^2).

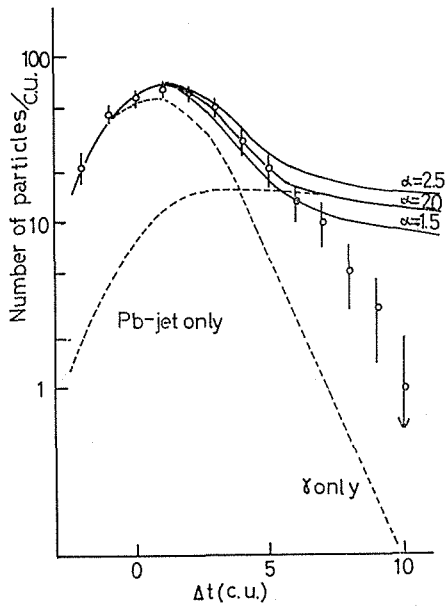

Fig. 7

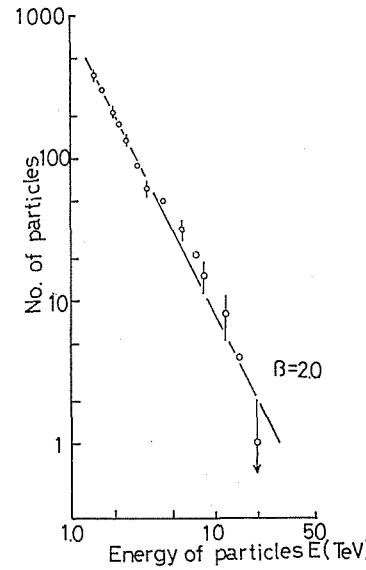

Fig. 8

Fig. 7. Expected curves of the differential starting point distribution of showers, in case that the fluctuation is given by the Gaussian distribution with $\sigma^2=3$ (see text). Dotted lines are calculated curves for the γ-rays and for the Pb-jets. Solid lines are for the total showers in case that the ratio α is 1.5 or 2.0 or 2.5. The open circles are the measured results in the thick part and only the statistical errors are considered.
From the figure, it is found that the α is given by 2.0 ± 0.5 and the showers which start below the depth 8 c.u. (mostly Pb-jets) are overlooked.

Fig. 8. Integral energy spectrum of the total showers observed in the thick part. The open circles are the measured values and only statistical errors are considerd. Ordinate is the number of observed showers and abscissa is the energy of shower.

4–1–2 The zenith angle distribution

We obtained 846 showers. With respect to energy, no detection loss is expected above 1.5 TeV. The number of showers with the energy above this threshold are 384. Figure 8 shows their energy spectrum.

The zenith angle distribution of the showers is shown in Fig. 9. It may be a function of ratio of the atmospheric depth x at an observation point to the attenuation mean free phth λ_a in the atmosphere. In Fig. 9–1, the dotted curves are the calculated result for various x/λ_a's. Comparison with the data shows that $x/\lambda_a=7.0\pm1.0$. On the other hand the zenith angle distribution is also represented by $\cos^n\theta$, $n=9.0\pm1.0$ (see Fig. 9–2). At moderate atmospheric depths, an approximate relation $n=2+(x/\lambda_a)$ should hold, the relation is actually satisfied in our

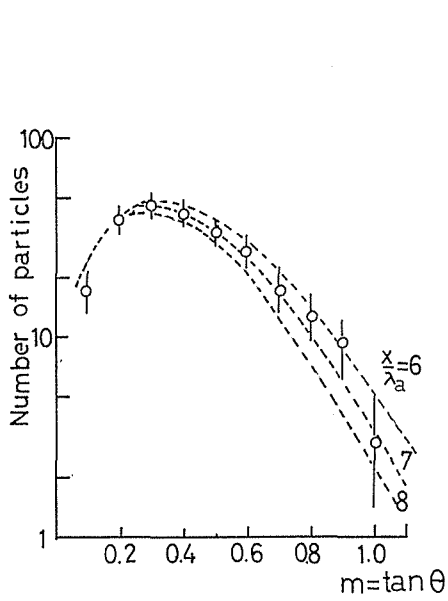

Fig. 9–1

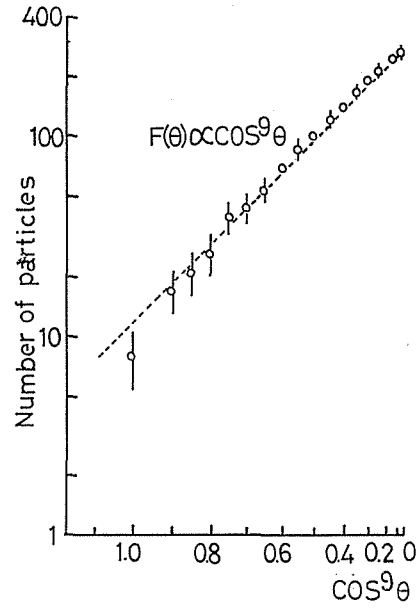

Fig. 9–2

Fig. 9. Zenith angle distribution for the total showers observed in the thick part.

9–1. Differential zenith angle distribution. Dotted line are the expected curves for the cases, $x/\lambda_a=6,7$ and 8 where x is the atomospheric depth of observation point and λ_a is the attenuation mean free path of γ-rays in the atomosphere (see text). The open circles are the measured results and only the statistical errors are considered. Abscissa is $m=\tan\theta$ where θ is the zenith angle.

9–2. Integral zenith angle distribution. Dotted line is given by $\cos^9\theta$. The open circles are the measured results and only the statistical errors are considered.

experiment. Thus the value of n determined here may be a good estimate.

Then the value of λ_a becomes about 93 g/cm^2. The EC constructed of iron (abbreviated by Fe-EC) were also exposed at Mt. Fuji. The Fe-EC group[8] reported a value, 95 ± 10 g/cm^2, in agreement with the present result.

4–1–3 Flux and energy spectrum

To obtain the verticla flux and energy spectrum, the next corrections and the solid angle have been considered.

Correction by Pb-jets The fraction K of the Pb-jets to the total showers which start within t c.u. from the top of EC is given by

$$K=\frac{\alpha(1-\exp(-t/30))}{1+\alpha(1-\exp(-t/30))},$$

where $\exp(-t)$ is assumed as far smaller than 1. In the present experiment almost all of showers were observed which start within the depth $t=8$ c.u. (see Fig. 8), and the ratio α may be put 2.0 ± 0.5. Thus we obtain $K=0.32\pm0.05$, i.e. the contribution of Pb-jets is 32% of the total showers. Thus the correction factor for

γ-ray flux, K_{Pb}, is 0.68*.

Effective area Among the incoming particles, some of them fall on a marginal zone or a side of one unit of EC (40 cm$\times$50 cm) and do not go through the whole thickness of the EC. As it is impossible to measure the energies of those particles

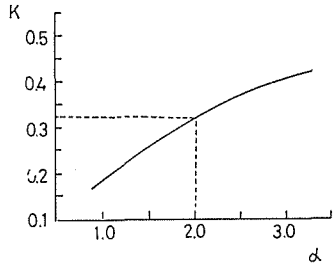

Fig. 10. Expected curve of the relation of the fraction, K, of the Pb-jets to the total showers and the ratio, α, of Pb-jets to γ-rays at the top of the chamber.
Dotted lines represent the case of our result, $\alpha=2$.

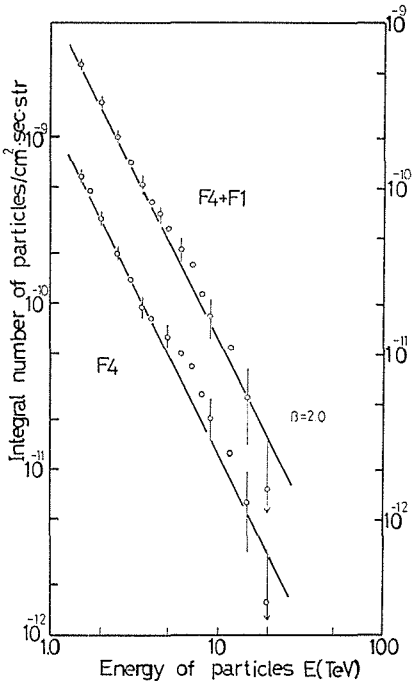

Fig. 11

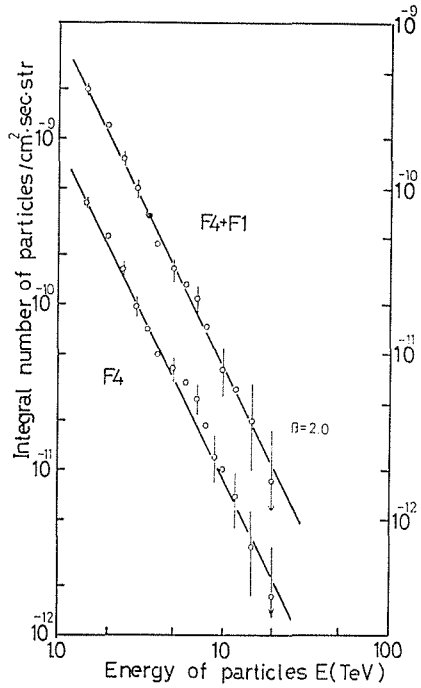

Fig. 12

Fig. 11. Integral vertical flux of γ-rays observed in the thick part and the Chamber FI. The open circles and the open circles with dots are the measured relults and the letter F4 denotes the result obtained only by the thick part of the Chamber FIV, and the letter F4+F1 denotes those obtained by the Chamber F1 and the thick part of the Chamber FIV. Left scale is for F4 and right scale for F4+F1. Errors are statistical only. Solid lines are the power spectrum, $E^{-\beta}$, with $\beta=2.0$.

Fig. 12. Integral vertical $S_{2\gamma}$ flux. (See text and the figure caption of Fig. 11).

* The K depends wearkly on t, for $\alpha=2.0$ K equals to 0.34 for $t=7$ and to 0.30 for $t=9$. Figure 10 shows the α dependence of K. K depends weakly also on α. Thus K is correct within 15% error.

with irregular traversal, they have to be omitted from the statistics. For this purpose, the marginal zone within 0.5 cm from the external edge of each blocks are eliminated from the statistical preparation. So the effective area is approximately 5% smaller than the real one, and the correction factor of effective area, K_s, is equal to 1.05.

Solid angle From the integral zenith angle distribution $\cos^n\theta$ with $n=9.0\pm 1.0$, the effective solid angle $2\pi/n$ is obtained to be $1/(1.43\pm 0.16)$ str.

Then we obtained the integral vertical flux of the total γ-rays (I) from the flux of all detected showers (J); $I=K_{Pb}\cdot K_S\cdot 1.43\cdot J$. Figure 11 shows the spectrum.

If high energy cosmic-ray particles interact with air nuclei near the chamber, a group of γ-rays and nuclear active particles may be observed in the same direction. These particles are called 'family' and its presence in a chamber sometimes brings about considerable fluctuation. For this reason, so called $S_{2\gamma}$ spectrum is used which is constructed as follows: Let the highest energy in a family be E_1 and the second highest be E_2. The $S_{2\gamma}$ spectrum at energy E is made up of all particles that satisfy $E_1>E>E_2$. This means that at $E<E_2$, the family dose not contribute any more to $S_{2\gamma}$. Single γ-ray is assumed to be a special case of a family in which E_2 is not observable.

The flux of γ-rays above 1.5 TeV, I_γ (1.5 TeV) is $5.9\pm 0.2\times 10^{-10}$/cm^2·sec·str and the corresponding flux of $S_{2\gamma}$ (Fig. 12), $I_{S2\gamma}$(1.5 TeV), is $4.1\pm 0.3\times 10^{-10}$/cm^2·sec·str. The two spectra are expressed by the simple power, $E^{-\beta}$, with the same exponent $\beta=2.0\pm 0.1$. The results agree well with the results of the Chamber F I and the Fe-EC. The Chamber F I gives; $I_\gamma(1.5\text{ TeV})=5.6\pm 0.4\times 10^{-10}$/cm^2·sec·str,

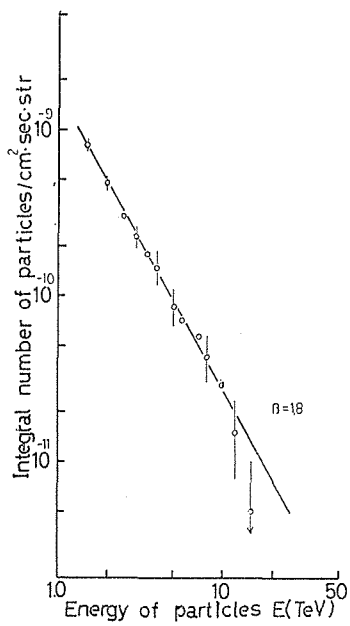

Fig. 13. Integral vertical flux of Pb-jets observed in the Chamber FI with thickness 50 c.u., 1.6 m^2 in area.
The open circles are the observed results and only the statistical errors are considered. Solid line shows the power spectrum, $E^{-\beta}$, with $\beta=1.8$.

$\beta=2.0\pm0.1$, and $I_{S2\gamma}(1.5\ \mathrm{TeV})=3.6\pm0.3\times10^{-10}/\mathrm{cm}^2\cdot\mathrm{sec}\cdot\mathrm{str}$, $\beta=2.0\pm0.1$. The Fe-EC gives $I_\gamma(1.5\mathrm{TeV})=6.0\pm0.5\times10^{-10}/\mathrm{cm}^2\cdot\mathrm{sec}\cdot\mathrm{str}$ and $\beta=2.2\pm0.2$.

For Pb-jets, we obtained, in the Chamber F I, a simple power spectrum (Fig. 13) with the exponent $\beta=1.8\pm0.2$ and the flux of $I_{\mathrm{Pb}}(1.5\ \mathrm{TeV})=8.2\pm0.5\times10^{-10}/\mathrm{cm}^2\cdot\mathrm{sec}\cdot\mathrm{str}$ which is to be compared with the Fe-EC* result: $I_{\mathrm{Fe}}(1.5\ \mathrm{TeV})=1.0\pm0.1\times10^{-10}/\mathrm{cm}^2\cdot\mathrm{sec}\cdot\mathrm{str}$ and $\beta=1.8\pm0.1$.

4–2 Thin part
—Energy region from 15 TeV to 100 TeV—

4–2–1 Secanning efficiency

To obtain the spectrum at higher energies, scanning was done in the thin part. Apart from 7 large families with total energy (ΣE_γ) greater than 200 TeV, 195 showers with energy greater than 10 TeV were obtained. In the 7 large families 83 showers with energy greater than 10 TeV were found. Figure 14 presents the total γ-ray spectrum. As shown in the figure, the detection bias is found in the energy region below 10 TeV. Because of the insufficient material thickness, the

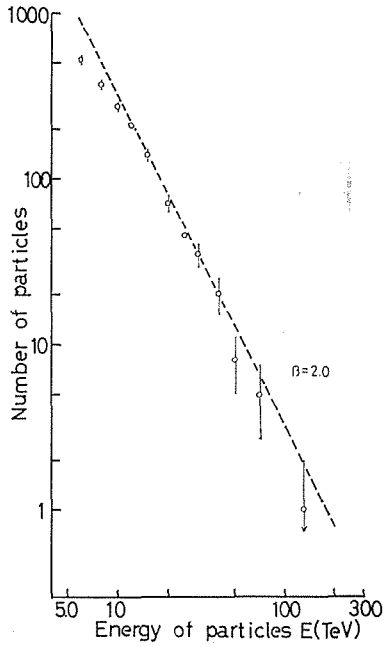

Fig. 14

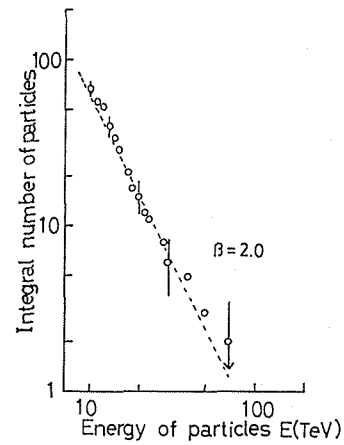

Fig. 15

Fig. 14. Integral energy spectrum for the total showers observed in the thin part. (Spacing factor is not calibrated.) The open circles are the measured results and only the statistical errors are considered. Dotted line shows the power spectrum, $E^{-\beta}$, with $\beta=2.0$.

Fig. 15. Integral energy spectrum of the showers with positive Δt value (see text) observed in the thin part. (Spacing factors is not calibrated.) The open circles are the measured results and only the statistical errors are considered. Dotted line shows the power spectrum, $E^{-\beta}$, with $\beta=2.0$.

* Iron is more efficient than lead for the observation of nuclear active particles, because the mean free path is about one third of that of lead.

development of shower is not so enough that the scanning efficiency is a very serious problem, while the contribution of Pb-jets is negligible. The following two corrections were considered.

Correction due to the shower development As shown in Fig. 3, optical densities of different energies are rather close to each other in early stages of shower development so that a number of showers might be overlooked in the thin part irrespective of energy. In Fig. 15, the integral spectrum of showers with positive Δt is shown. It is expressed by a simple power spectrum, which implies that there is no detection bias depending on energy.

In order to estimate the detection probability of the showers in the thin part we compared the integral distribution of the starting points observed in the thick part (dotted curve in Fig. 16) with that in the thin part (solid curve in Fig. 16). The difference in the region of positive Δt is due to the overlooking of early stage showers in the thin part. Thus we obtain the correction factor $K_t=1.4$ (=235/165) independent of shower energy.

Figure 17 shows a relation of K_t and Δt which is calculated by assuming that all showers that start before the depth Δt are detectable. Here the starting fluctuation is not considered. The Δt is, however, never smaller than 1.0, so the accuracy of K_t is within 15% error.

Detection bias due to the effective thickness of the materials Figure 18 shows the energy spectrum of the showers with large value of $m=\tan\theta$ (greater than 0.5

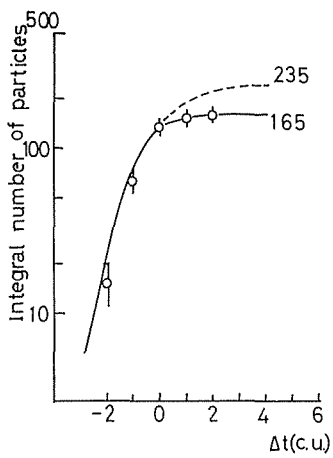

Fig. 16

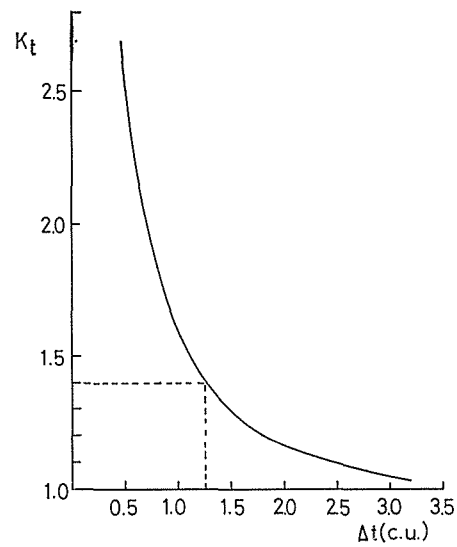

Fig. 17

Fig. 16. Integral starting point distribution of the showers observed in the thin part. The open circles are the measured results and solid line is a best fit curve to the data. Dotted is the expected curve from the data in the thick part. (See Fig. 7.) The 235 particles are expected but only the 165 particles are observed. Abscissa is the starting point Δt.

Fig. 17. Calculated curve of the dependence on the depth Δt, of the correction factor, K_t, due to overlooking of showers in their early stages in the thin part. Here we assume that all showers which start within Δt c.u. are detectable. Dotted lines represent the case of our result, $K_t=1.4$.

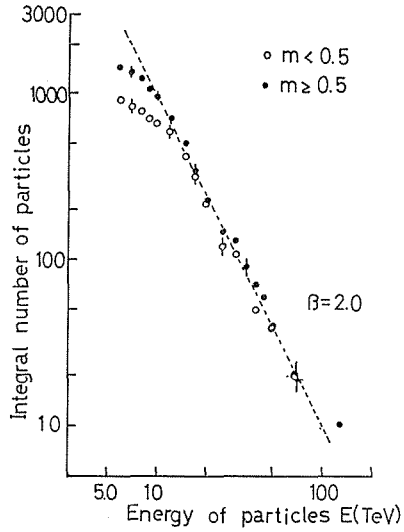

Fig. 18. Integral energy spectra of the showers with $m=\tan\theta$ smaller than 0.5 and greater than or equal to 0.5. (Spacing factor is not calibrated.)
The open circles are the measured results of the showers for the former case and the dots for the latter case. Dotted line is the power spectrum, $E^{-\beta}$, with $\beta=2.0$. Only the statistical enors are considered.

i.e. zenith angle θ is greater than 26.6°) and that of small m. The spectrum of the showers with small m deviates from simple power spectrum below 15 TeV. This is because, for such showers, the effective material thickness is so thin that shower development is not enough.

4-2-2 Flux, energy spectrum and zenith angle distribution

The zenith angle of 135 showers with the energy greater than 15 TeV can be fitted by calculation with a parameter $x/\lambda_a=6.5$ or $n=8.5\pm1.5$. Then λ_a is, obtained as 100 ± 20 g/cm^2 which agrees well with the result in the thick part. Considering the corrections above mentioned, the vertical flux and the energy spectrum in the thin part* are obtained by the same manner as in the thick part and found to be:

$$I_\gamma(>E)=I_\gamma(15\text{ TeV})\times(E/15)^{-\beta},$$
$$I_\gamma(15\text{ TeV})=5.4\pm0.5\times10^{-12}/\text{cm}^2\cdot\text{sec}\cdot\text{str}, \qquad \beta=2.0\pm0.2.$$
$$I_{S2\gamma}(>E)=I_{S_2\gamma}(15\text{ TeV})=\times(E/15)^{-\beta},$$
$$I_{S2\gamma}(15\text{ TeV})=3.0\pm0.6\times10^{-12}/\text{cm}^2\cdot\text{sec}\cdot\text{str}, \qquad \beta=2.05\pm0.20.$$

* The radiation process in high energy, as is well known, suffers significant effect which is called as the Landau, Pomerachuk and Migdal effect[9], which causes the reduction of the cross section for these processes compared with the Bethe-Heitler cross section. Cascade shower theory which treats this effect exactly has not yet been obtained.

According to the preliminaly result by one-dimensional Monte Carlo simulation[10], this effect makes shower develop more slowly and as the primary energy increases, the effect of the penetration of cascade shower increases. So, in the thin part, the energy of shower might be overestimated slightly, and the spectrum might be possibly steeper a little. The exact quantitative treatment remains to be done in future.

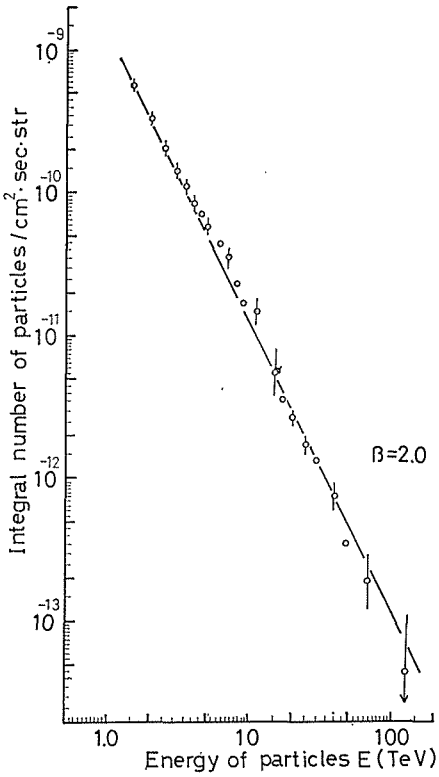

Fig. 19

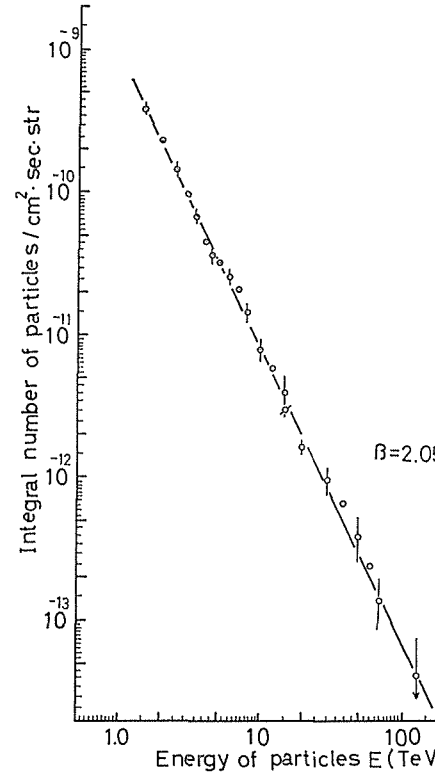

Fig. 20

Fig. 19. Integral vertical flux of the total γ-rays.
The open circles are the measured results of γ-rays observed in the thin part and the circles with dots are those of γ-rays observed in the thick part and the Chamber FI. Only the statistical errors are considered. Solid line show the power spectrum, $E^{-\beta}$, with $\beta=2.0$. (Spacing factor is calibrated.)

Fig. 20. Integral vertical $S_{2\gamma}$ flux (see text and figure caption of Fig. 19).

(See Fig. 19 and 20.).

4–2–3 Comparision of the energy spectra in the two energy region

As shown in Fig. 19 and 20, the energy spectra obtained in the thick part and in the thin part are connected smoothly at about 15 TeV. The spectra are well expressed by a simple power up to 100 TeV. This suggests also the correctness of our new method of energy determination mentioned in Section 3.

Summing these, we obtain:

$$I_\gamma(>E)=5.9\pm0.2\times10^{-10}(E/1.5)^{-2.0\pm0.1}/\mathrm{cm}^2\cdot\mathrm{sec}\cdot\mathrm{str}\,,$$

$$I_{S\gamma2}(>E)=4.1\pm0.3\times10^{-10}(E/1.5)^{-2.05\pm0.10}/\mathrm{cm}^2\cdot\mathrm{sec}\cdot\mathrm{str}\,.$$

5. Discussions

We now compare our results with those of the Chacaltaya EC and the Norikura EC experiments. The results of the respective experiments are;

Mt. Chacaltaya (5200 m)[9]

$$I_\gamma(>E)=2.5\pm0.1\times10^{-9}(E)^{-2.05\pm0.05}/\mathrm{cm}^2\cdot\mathrm{sec}\cdot\mathrm{str} \quad \text{(in TeV)},$$

Mt. Norikura (2800 m)[2]

$$I_\gamma(>E)=5.0\pm0.6\times10^{-9}(E)^{-2.3\pm0.2}/\mathrm{cm}^2\cdot\mathrm{sec}\cdot\mathrm{str} \quad \text{(in TeV)},$$

(See also Fig. 21.).

The value of the exponent in the Mt. Norikura experiment seems to be different form the two results. Because of poor statistics, the result should not be taken into account with the same weight. We conclude that the value of the exponent of γ-ray spectrum is nearly constant in a deeper region of the atmosphere (where the equilibrium of nuclear active particles and γ-rays is approximately established) and does not depend on the energy up to 100 TeV.

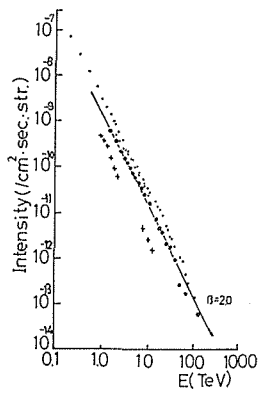

Fig. 21

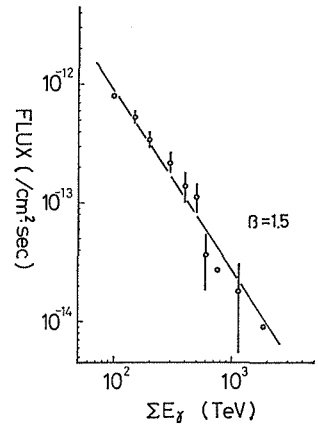

Fig, 22

Fig. 21. Comparision of the integral vertical flux of total γ-rays.
The dots are the measured results in the Chacaltaya experiment, the daggers are those in the Norikura experiment and the open circles are ours. Solid line is the power spectrum, $E^{-\beta}$, with $\beta=2.0$.

Fg. 22. Integral energy flow spectrum of the γ-ray families observed in the Chambers FIII, FIV and FV. (Spacing factor is not calibrated.)
The open circles are the measured results and only the statistical errors are considered. Solid line is the power spectrum, $E^{-\beta}$, with $\beta=1.5$.

Figure 22 shows the energy spectrum of the large families with total energy greater than 100 TeV. It is also represented by a simple power spectrum with $\beta=1.5$ up to 1000 TeV.

Two important phenomenological results[12),13)] for multi-particle production which previously were asserted by cosmic-ray physists, were recently confirmed with more accuracy by accelerators. They are the rising total cross section of p-p interactions[14)] (mainly in the inelastic part) and the Feynman scaling for the inclusive distribution[15)].

Many authors[16)] have discussed about these asymptotic behaviors in cosmic-ray energy region. From our data, we shall breifly mention about those. Detailed discussions will be found in ref. 17.

Scaling hypothesis[18)] The hypothesis postulates that the production spectrum of the secondary particles does not depend on the initial energy E_0 and the sec-

ondary particle energy E_s separately, but does only on the energy ratio E_s/E_0 (i.e. so called Feynmam scaling variable $x=2P_{11}/\sqrt{s}\cong E_s/E_0$) in the asymptotic energy region. If the hypothesis is valid, the exponent of the spectrum of γ-rays and that of Pb-jets sould be same and they are equal to the exponent of the primary cosmic-ray spectrum. But as shown in §4, the exponents of the Pb-jet spectrum and γ-ray spectrum are given by about 1.8 and 2.0, respectively. The exponent of the primary spectrum obtained by EAS experiments is about 1.7 in our energy region[19]. So we would suggest that the scaling hypothesis probably breaks down in the energy region above several 10 TeV*. The breakdown may be caused, for example, by the production of giant fireballs, resulting in the decrease of the leading particle i.e. a strong violation of scaling in the fragmentation region[21].

Rising total cross section From the value of λ_a, we obtain the absorption cross section $\sigma_{p-\mathrm{air}}$ as shown in Appendix 2. Its value is found to be about 330 mb from the altitude valiation of γ-ray flux and about 390 mb from the zenith angle distribution. They can be compared directly with the value of $\sigma_{p-\mathrm{air}}$, 320 ± 30 mb, at 19.3 GeV by CERN-PS[22]. There wowld be a possible increase of $\sigma_{p-\mathrm{air}}$ from 19.3 GeV to the energy region above 10 TeV.

At the end we report a curious feature for very high energy γ-rays. We have four γ-rays with energy greater than 50 TeV. Each of these γ-rays belongs to different families. In these families, there are only a few accompaning γ-rays with the energy greater than 10 TeV. Especially, a γ-ray with the highest energy (130 TeV) has no accompaning γ-rays except only one sevaral TeV γ-ray. These events can not be considered as products of the conventional fireball but are expected to be those from a excited baryon or the coherent production. This type of events will give important information about the nature of the excited baryon.

Appendix 1 Effects of the accuracy of energy determination on the absolute value of the flux.

Systematic error If the measured value of energy, E, is A times the true value, E_0, the absolute flux is A^β times the true one, where β is the exponent of the spectrum. In the present experiment we use the optical densities, which may vary under different expreiment conditions, and should be calibrated by track counting. As seen from Fig. 2 and Fig. 6, we can see there is no systematic error and therefore the absolute value obtained by the optical density measurement can be directly compared with that[23] obtained by track counting.

Statistical error Because of the steepness of the energy spectrum, the statistical error may affect the absolute value of flux.

Let the true differential energy spetcrum be $I(E_0)=I_0\beta E_0^{-\beta}(dE_0/E_0)$. The statistical error is assumed to be represented by a Gaussian function;

$$f(x)dx=\frac{1}{\sqrt{2\pi}\sigma}e^{-x^2/2\sigma^2}dx\,, \qquad \text{(A1-1)}$$

* Monte Calro simulation[20] of the diffusion of γ-rays in the atmosphere were done with the assumption that the secondary pions are produced by fire balls. According to this simulation, the observed energy of γ-rays are smaller than the one-tenth of energy at interactions. So the γ-rays with energy greater than 1 TeV are the products of the interactions at energies greater than 10 TeV.

where $x=(E_0-E)/E_0$. Then the measured energy spectrum will be

$$dE\iint\delta(E-(1-x)E_0)f(x)I(E_0)dE_0dx\cong\left[1+\frac{\sigma^2}{2}\beta(\beta+1)\right]I(E)dE\,. \tag{A1-2}$$

In our experiment, we have $\sigma\sim0.2$ and $\beta=2.0$ which entails only 4% error.

Appendix 2 The relation between attenuation mean free path and absorption cross section ($\sigma_{p-\mathrm{air}}$).

If the collision mean free path of the nucleon is λ_N, the relation between λ_a and λ_N is given as follows. The diffusion equation of the nucleons in the atmosphere may be written as

$$\frac{\partial F_N(E,x)}{\partial x}=-\frac{1}{\lambda_N}F_N(E,x)\int_0^1 f_N(\eta)d\eta+\frac{1}{\lambda_N}\int_0^1 F_N\left(\frac{E}{1-\eta},x\right)\frac{f_N(\eta)}{1-\eta}d\eta\,, \tag{A2-1}$$

where $F_N(E,x)$ is the flux of nucleons at the depth x, η is the inelasticity coefficient at the collision of a nucleon with air nucleous and $f_N(\eta)$ is its distribution function.

This equation can be solved generally by use of the Laplace and the Mellin transformations. In case of the power spectrum, the solution is obtained easily. Putting the function $E^{-(\beta+1)}\exp(-x/\lambda_a)$ into the equation, we obtain

$$\frac{1}{\lambda_a}=\frac{1}{\lambda_N}\left\{1-\int_0^1 d\eta f_N(\eta)(1-\eta)^\beta\right\}\,. \tag{A2-2}$$

If the uniform distribution of η is assumed ($f_N(\eta)=1$)[24], the bracket on the right hand side becomes $\beta/(\beta+1)$. For $\beta=2$, we obtain $\lambda_N=\frac{2}{3}\times\lambda_a$. Thus the relation between λ_a and $\sigma_{p-\mathrm{air}}$ is

$$\sigma_{p-\mathrm{air}}(mb)=2.4\times10^4/\lambda_N(\mathrm{g/cm^2})=3.6\times10^4/\lambda_a(\mathrm{g/cm^2})\,. \tag{A2-3}$$

If the total or inelastic cross section is wanted, the inelasticity distribution of the corresponding process must be used. We have neglected the diffraction peak at $\eta\sim0$, so the above cross section is nearly equal to the absorption corss section.

Since the experiment was done at the mountain altitude, the γ-rays and nucleons can be regarded in the equilibrium state. If they have a common value for their attenuation length, we can obtain $\sigma_{p-\mathrm{air}}$ from the eq. (A2-3). (Here we neglect the $\pi^{\pm}$-on contaminations. If we consider this effect correctly, $\sigma_{p-\mathrm{air}}$ is given by larger value.) From the zenith angle distribution above 1.5 TeV, $\sigma_{p-\mathrm{air}}$ is about 390 mb, and from altitude valiation by comparision with data at Mt. Chacaltaya and at Mt. Norikura, $\sigma_{p-\mathrm{air}}$ is about 330 mb.

ACKNOWLEDGEMENT

The author would like to express his sincere thanks to Prof. H. Hasegawa for his kind help in writing the manuscript and valuable comments.

He is also wish to express his thanks to Prof. I. Mito and Drs. K. Kasahara and A. Ohsawa for their continuous encouragements and guidances through the work. He is deeply grateful to Profs. I. Ohta and T. Yuda and Dr. Takahashi for their advices. Thanks are also due to the members of Cosmic Ray Division B of Institute for Nuclear Study for their helpful supports.

REFERENCES

1) I. Ohta, K. Kasahara, I. Mito, A. Ohsawa, T. Taira, and S. Torii, in Proceedings of the thirteenth International Conference on Cosmic Rays, Denver, 1973, Vol. 3, P. 2250; I. Ohta, K. Kasahara, A. Ohsawa, I. Mito, and S. Torii, in Proceedings of International Cosmic Ray Symposium on High Energy Phenomena, Tokyo, 1974, P. 33.
2) M. Akashi, Z. Watanabe, A. Misaki, I. Mito, Y. Oyama, S. Tokunaga, T. Ogata, Y. Tsuneoka, S. Dake, K. Yokoi, S. Hasagawa, J. Nishimura, K. Niu, T. Taira, A. Nishio, Y. Fujimoto and N. Ogita, Prog. Theor. Phys. Supple. No. 32 (1964), 1.
3) I. Ohta, Prog. Theor. Phys. Supple. No. 47 (1971), 271; I. Ohta, K. Kasahara, T. Kobayashi, E. Mikumo, I. Mito, A. Ohsawa, K. Sato, M. Tsujikawa, S. Uchida and S. Torii, in Proceedings of International Cosmic Ray Symposium on High Energy Phenomena, Tokyo, 1974, P. 103.
4) J. Nishimura, Prog. Theor. Phys. Supple. No. 32 (1964), 72.
5) M. Hazama and K. Nishikawa, in Proceedings of International Cosmic Ray Symposium on High Enekgy Phenomena, Tokyo, 1974, P. 72.
6) A. P. Chubenko, T. A. Ershova, R. A. Nam, S. I. Nikolsky, V. P. Pavljutchenko, Y. N. Stamenov and V. I. Yakovlev, in Proceedings of the thirteenth international Conference on Cosmic Rays, Denver, 1973, Vol. 3, P. 2191.
7) Japanese and Brazilian Emulsion Chamber Group, SJC-P-66-1 (1966).
8) T. Shirai, T. Yuda, M. Shibata and K. Taira, in Proceedings of International Cosmic Ray Symposium on High Energy Phenomena, Tokyo, 1974, p. 39.
9) L. D. Landau and I. Yu. Pomeranckuk, Dokl. AN SSSR, **92** (1953), 535, 735; A. B. Migdal, Zh. Experim. Teo. Fig., **32** (1957), 633.
10) A. Misaki, K. Mori, M. Shibata, T. Shirai and T. Yuda, in Proceedings of International Cosmic Ray Symposium on High Energy Phenomena, Tokyo, 1974, P. 142.
11) E. Konishi, T. Shibata, E. H. Shibuya, and N. Tateyama, CKJ-Report-9, Cosmic Ray Laboratory, University of Tokyo (1971).
12) V. V. Akimov, N. L. Grigorov, N. A. Mamotuva, V. E. Nesterov, V. L. Prokhin, I. D. Rapoport and I. A. Savenko, in Proceedings of the eleventh International Conference on Cosmic Rays, Budapest, 1969, Vol. 3, P. 211.
13) C. M. G. Lattes, M. S. M. Mantovani, C. Santos, E. H. Shibuya, Armando Trtelli Jr., N. M. Amato, A. M. F. Endler, M. A. B. Bravo, C. Aguirre, M. Akashi, Z. Watanabe, I. Mito, K. Niu, I. Ohta, A. Ohsawa, T. Taira, J. Nishimura, Y. Fujimoto, S. Hasegawa, K. Kasahara, E. Konishi, T. Shibata, N. Tateyama, No. Ogita, Y. Maeda, K. Yokoi, Y. Tsuneoka, A. Nishio, T. Ogata, M. Hazama, K. Nishikawa, Y. Oyama and S. Dake, Prog. Theor. Phys. Supple. No. 47, 1.
14) U. Amaldi et al., Phys. Lett. **43B** (1973), 231; U. Amaldi et al., Phys. Lett. **44B** (1973), 112. S. R. Amendolia et al., Phys. Lett. **44B** (1973), 119.
15) C. L. Wang, Phy. Rev. **D7** (1973), 2609.
16) For example, G. B. Yodh, Yash Pal and J. S. Trefil, Phy. Rev. Lett. **28** (1972), 1005; W. R. Frazer, C. H. Poon, Dennis Silverman and Harry J. Yesian, Phys. Rev. **D5** (1972), 1953.
17) K. Kasahara and Y. Takahashi, in Proceedings of International Cosmic Ray Symposium on High Energy Phenomena, Tokyo, 1974, P. 85.
18) R. P. Feynman, Phy. Rev. Lett. **23** (1969), 1415.
19) M. Nagano, in Proceedings of Synposium on Cosmic Rays, Cosmic Ray Laboratory, University of Tokyo, (1974). (in Japanese); N. L. Grigorov, I. D. Rapoport, I. A. Savenko, V. E. Nesterov and V. L. Prokhin, in Proceedings of the twelfth International Conference on

Cosmic Rays, Hobart, 1971. Vol. 1, P. 172.

20) Y. Fujimoto, S. Hasegawa, K. Kasahara, N. Ogita, A. Ohsawa and T. Shibata, Prog. Theor. Phys. Supple. No. 47 (1971), 246.

21) Ref. 13 and N. L. Dobrotin, in Proceedings of the twelgth International Conference on Sosmic Rays, Hobart, 1971, Invited and Rapporteur papers, P. 308.

22) G. Belletini, G. Cocconi, A. N. Diddens, E. Lillethan, G. Matthiae, J. P. Scanbon and A. M. Wetherell, Nuclear Phys. **79** (1966), 609; A. Liland and H. Pilkuhn, in Proceedings of the eleventh International Conference on Cosmic Rays, Budapest, 1969, Vol. 3, P. 293.

23) J. Nishimura, Handbuch der Physik 46/2 (Springer-Verlag, Berlin, 1967), 1; J. Nishimura, and K. Kmata, Prog. Theor. Phys. Supple. No. 6 (1968), 93.

24) G. W. Mason and J. W. Elbert, in Proceedings of the thirteenth International Conference on Cosmic Rays, Denver, 1973, Vol. 3, P. 2348; CHLM Collaboration, as cited in R. Slansky, Phy. Rep. 11 No. 3(1974), 99.